

Tuning of Elliptic Whispering-Gallery-Mode Microdisk Waveguide Filters

Svetlana V. Boriskina, *Member, IEEE*, Trevor M. Benson, *Senior Member, IEEE*, Phillip Sewell, *Member, IEEE*, and Alexander I. Nosich, *Senior Member, IEEE*

Abstract—High- Q semiconductor microdisk resonators laterally coupled to optical waveguides serve as compact and robust components in wavelength-division-multiplexing systems. We present an efficient algorithm for the two-dimensional design of wavelength-selective filters based on waveguide-coupled whispering-gallery-mode (WGM) microresonators of arbitrary cross-sectional shape. A full-wave integral equation formulation enables us to accurately account for the coupling between the resonator and bus waveguide as well as for radiation and material losses. Furthermore, we apply this approach to the analysis of elliptic-resonator filters. Filter tuning by changing the resonator shape from circular to elliptic reduces the dependence of the coupling efficiency on the width of the air gap. Two alternative coupling designs are suggested for monolithic and hybrid integration technologies. One is based on increasing the coupling length, while the other exploits the field concentration at the increased-curvature portion of the deformed WGM resonator.

Index Terms—Elliptic microresonator, integral equations, monolithic and hybrid integrated circuits, optical filters, wavelength-division multiplexing (WDM), whispering-gallery modes (WGMs).

I. INTRODUCTION

CIRCULAR whispering-gallery mode (WGM) resonators are known as versatile elements in photonics with applications including multiplexers, modulators, selective and tunable filters, add/drop filters, ultracompact optical and microwave oscillators, and semiconductor lasers [1]–[6]. Their high-quality factor, along with the simplicity with which they can be fabricated, makes WGM microdisk resonators attractive for use in all-optical systems for a wide range of wavelengths and materials.

High-index-contrast semiconductor microresonators, characterized by a strong lateral confinement of the field, provide advantages for high-density integration with other semiconductor components. They do not require facets or gratings for optical feedback and thus are particularly suited for monolithic integration. Monolithic (GaAs- or InP- based) integration of optical elements on a single semiconductor substrate enables

the fabrication of low-cost high-performance compact optoelectronic integrated circuits. However, a very important and costly issue in highly confined monolithic systems is optical coupling. The strong optical field confinement and small coupling interaction lengths between circular microresonators and planar waveguides require using small air gaps, which are difficult to fabricate. One of the ways to achieve the desired level of coupling with a wider air gap is to increase the coupling interaction length by either curving the adjacent waveguide along the microdisk [4], [7], [8] or to use WGM elliptic and racetrack resonators [7]–[10] coupled to a waveguide along their major axes.

In addition to III–V semiconductor-based integration technologies, several approaches based on different material systems exist. The most popular are hybrid planar lightwave circuits (PLCs): planar silica or polymer-waveguide networks on a silica substrate, on which different optical devices are assembled [11]. Compared with semiconductor waveguides, polymer waveguides show lower absorption losses, higher tunability, better matching to optical fibers, and better temperature stability. However, in this case, the effective refractive indexes of the dielectric waveguide and semiconductor microdisk are not matched, which may lead to the excitation of parasitic higher order resonances in the microdisk [5].

A number of simple physical models have been developed for evanescent coupling from optical waveguides into circular and deformed WGM resonators. They include circuit models [1], approaches based on the coupling of modes in space [2] and time [3], conformal transformation methods [7], and beam propagation methods (BPMs) [2]. Although the results obtained from these methods give a physical picture of the coupling mechanism and offer ideas for alternative filter designs, they are based on approximate solutions. There is also a clear need for design tools with a high and controlled accuracy, which are based on reliable analytical methods. Versatile and accurate numerical methods, such as the finite-difference time-domain (FDTD) method [4], [6] can be applied in general for the analysis for any complicated optical structure, although they are time and memory consuming and can fail to give a correct description of the high- Q WGM resonances [12].

(*) see comment below

In this paper, we present an accurate and robust numerical analysis of arbitrary-shaped waveguide-coupled microdisks by using a combination of two accurate mathematical techniques. First, the Green's function method is applied to derive the set of the contour integral equations (IE) and then the method of analytical regularization (MAR) [13], [14] to convert them to a matrix equation with favorable features. The Green's function

Manuscript received December 26, 2002; revised May 7, 2003. This work was supported in part by the Engineering and Physical Sciences Research Council (EPSRC) under Research Grant GR/R65213.

S. V. Boriskina, T. M. Benson, and P. Sewell are with the School of Electrical and Electronic Engineering, University of Nottingham, Nottingham NG7 2RD, U.K. (e-mail: eezsb@gwmail.nottingham.ac.uk).

A. I. Nosich is with the Institute of Radio Physics and Electronics, National Academy of Sciences of Ukraine, Kharkov 61085, Ukraine (e-mail: alex@emt.kharkov.ua).

Digital Object Identifier 10.1109/JLT.2003.815497

gives a complete description of the layered host media and accurately accounts for the far-field radiation as well as the surface waves supported by the waveguide. The formulation of the problem in terms of the contour IEs enables the accurate shape-tuning of the microdisk without introducing staircasing errors usually associated with the FDTD analysis. Therefore, a stable and accurate numerical algorithm developed enables us to show how the coupling coefficient can be increased and parasitic resonances suppressed by modifying the shape of the microdisk and choosing the proper coupling configuration.

The remainder of the paper is organized into four sections. In Section II, we first sketch the development of the boundary IEs and discuss the singularities of the Green's functions that form the kernels of the IEs. Then, we present the algorithm for converting singular IEs into a matrix equation of the Fredholm second kind, which can be solved numerically with high and controllable accuracy. Finally, the expressions for the filter far-field characteristics are given. In Section III, we apply the method developed to the simulation of wavelength-selective waveguide-coupled microresonator filters, keeping a uniform accuracy of 10^{-4} . Overall, the full-wave electromagnetic approach used enables us to accurately account for the complex interactions between the microdisk and the waveguide and therefore develop the strategies for optimizing the filter performance. Finally, conclusions are drawn in Section IV.

II. PROBLEM FORMULATION AND METHOD OF SOLUTION

A. Waveguide-Coupled Microresonator Geometry and Scattering Problem Formulation

We consider a two-dimensional (2-D) microresonator having a refractive index n_r , coupled via an air gap of width w to a straight plane waveguide of thickness d and refractive index n_w , which serves as an evanescent wave input coupler. The microdisk cross section S is bounded by an arbitrary smooth closed curve L , described parametrically as $L : x = x(t), y = y(t), 0 \leq t \leq 2\pi$.

The resonator is excited by a guided surface wave incident from the left. After coupling to the microdisk, the incident wave power is partially carried along the waveguide in the form of transmitted wave(s), partially reflected backward in the form of reflected wave(s) and partially lost in the form of free-space radiation. For clarity of notation, we shall use the term *wave* to characterize a particular natural guided mode of the uniform waveguide, while the term *mode* will refer to a particular natural oscillation of the resonator. Two polarizations are considered: TE(H) having the electric field parallel to the $x - y$ plane of the microdisk cross section, and TM(E) having the electric field normal to this plane. Depending on the polarization, the total field can be uniquely determined from one component, H_z or E_z , respectively, which can be written as

$$U = \begin{cases} U^{\text{inc}} + U^{\text{sc}}, & \vec{r} \notin S \\ U^{\text{res}}, & \vec{r} \in S \end{cases}. \quad (1)$$

This function must satisfy the appropriate Helmholtz equation with corresponding coefficients in each material, the continuity

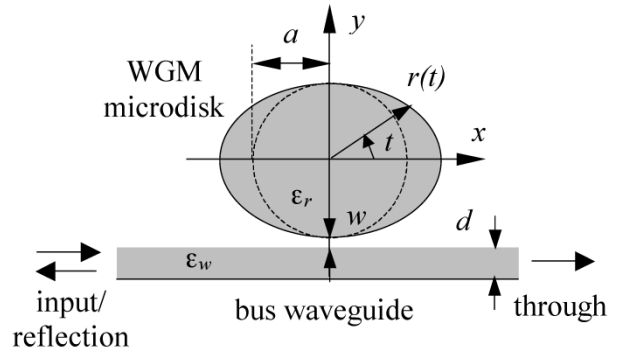


Fig. 1. 2-D WGM dielectric resonator laterally coupled to a planar dielectric waveguide.

conditions on the contour L and at the waveguide boundaries, and the modified radiation condition

$$U^{\text{sc}}(\vec{r}) \underset{r \rightarrow \infty}{\approx} \sqrt{\frac{2}{i\pi k r}} e^{ikr} \begin{cases} \Phi^{E(H)}(\varphi), & y > -b \\ 0, & -(b+d) < y < -b \end{cases} + \sum_{n=1(Q^{E(H)})} \begin{cases} T_n^{E(H)} - \delta_{nq}, & x > 0 \\ R_n^{E(H)}, & x < 0 \end{cases} V_n^{E(H)}(y) e^{ih_n|x|}. \quad (2)$$

Here, δ_{nq} is the Kronecker delta; $b = w + a$; and the q th incident wave is considered, $1(0) \leq q \leq Q^{E(H)}$, where $Q^{E(H)}$ is the total number of the guided waves supported by the waveguide at the given frequency. The superscript $E(H)$ denotes E(TM) or H(TE)- polarization, respectively. The function $\Phi^{E(H)}(\varphi)$ is the far-field radiation pattern of the resonator, $T_n^{E(H)}$ and $R_n^{E(H)}$ are the transmission and reflection coefficients of the n th guided wave of wavenumber h_n , and the functions $V_n^{E(H)}(y)$ are transverse-wave functions of the waveguide n th surface wave. Throughout the paper, the time-dependence convention $\exp\{-i\omega t\}$ is adopted and omitted for clarity.

B. Singular Contour Integral Equations and Their Analytical Regularization

The fields in every region of Fig. 1 can be expressed in terms of the single-layer surface potentials on the microdisk cross-sectional contour L [15]. A set of the first-kind singular IEs can be obtained imposing the tangential field continuity conditions at the contour L , as follows:

$$\int_L \varphi^{E(H)}(\vec{r}_s) G_r^{E(H)}(\vec{r}, \vec{r}_s) dl - \int_L \psi^{E(H)}(\vec{r}_s) G_w^{E(H)}(\vec{r}, \vec{r}_s) dl = U^{\text{inc}}(\vec{r}) \quad (3)$$

$$\frac{\partial}{\partial n} \left\{ \frac{1}{\alpha^{E(H)}} \int_L \varphi^{E(H)}(\vec{r}_s) G_r^{E(H)}(\vec{r}, \vec{r}_s) dl - \int_L \psi^{E(H)}(\vec{r}_s) G_w^{E(H)}(\vec{r}, \vec{r}_s) dl \right\} = \frac{\partial}{\partial n} U^{\text{inc}}(\vec{r}). \quad (4)$$

Here, $\partial/\partial n$ is the outer normal derivative to the contour, $\alpha^E = 1$, $\alpha^H = \epsilon_r$, and \vec{r} and \vec{r}_s indicate the observation and the source

points in the $x - y$ plane. The problem unknowns are the potential densities $\varphi(\vec{r}_s)$ and $\psi(\vec{r}_s)$. The kernel functions G_r and G_w are the Green's functions of the 2-D Helmholtz equation for a uniform medium of permittivity ε_r and the layered host medium, respectively. The latter Green's function accurately accounts for the field continuity on the dielectric interfaces parallel to the x axis as well as the far-field radiation conditions.

The 2-D Green's functions G_r and G_w are known to have logarithmic singularities at $\vec{r} \rightarrow \vec{r}_s$, while their normal derivatives are regular on smooth contours. Therefore, direct application of a discretization technique such as the Method of Moments will lead to poorly converging algorithms. To handle efficiently the singular parts of the kernels of IEs, we apply the procedure based on the integral operator (IO) regularization by the extraction and analytical inversion of the IO singular part that has an explicit solution in terms of Fourier series [13]. In this paper, to regularize the arbitrary-shape resonator singular IEs, we add and subtract an IO corresponding to a waveguide-coupled circular cylinder of radius a . It has the same type of logarithmic singularity at $\vec{r} \rightarrow \vec{r}_s$ as the original operator, and the solution for this problem has already been obtained [5].

First, we expand the unknown functions in (3) and (4) in terms of the Fourier series as follows (the superscript $E(H)$ is omitted):

$$\varphi(t_s)L(t_s) = \frac{2}{i\pi} \sum_{n=-\infty}^{\infty} \varphi_n e^{int_s}, \quad \psi(t_s)L(t_s) = \frac{2}{i\pi} \sum_{n=-\infty}^{\infty} \psi_n e^{int_s}. \quad (5)$$

Here, $L(t_s)$ is the Jacobian of the contour L , and similar expansions are written for the kernel and right-hand-side functions of (3) and (4). After performing the adding and subtracting procedure, the kernels consist of the sum of the singular waveguide-coupled circular-cylinder kernel and a regular function obtained as the difference between the original and subtracted kernels. Then, using angular exponents $\{e^{imt}\}_{m=-\infty}^{\infty}$, which are the orthogonal eigenfunctions of all the integral operators in (3) and (4), as a global basis in the Galerkin scheme, we combine the discretization and analytical regularization of IEs in one procedure. Thus, the set of singular IEs is reduced to the block-matrix equation

$$\begin{aligned} & \varphi_m H_m^l(k_r a) - \psi_m H_m^l(ka) J_m(ka) \\ & + \sum_{n=-\infty}^{\infty} A_{mn}^{\text{shape}} \varphi_n - \sum_{n=-\infty}^{\infty} (B_{mn}^{\text{slab}} + B_{mn}^{\text{shape}}) \psi_n = e_m \end{aligned} \quad (6)$$

$$\begin{aligned} & \varphi_m \frac{k_r a}{\alpha} H_m^l(k_r a) J_m'(k_r a) - \psi_m k a H_m^l(ka) J_m'(ka) \\ & + \frac{\sqrt{\varepsilon_t}}{\alpha} \sum_{n=-\infty}^{\infty} C_{mn}^{\text{shape}} \varphi_n - \sum_{n=-\infty}^{\infty} (ka D_{mn}^{\text{slab}} + D_{mn}^{\text{shape}}) \psi_n = \tilde{e}_m \end{aligned} \quad (7)$$

where k is the free-space wavenumber $k_r = k\sqrt{\varepsilon_r}$, $J_m(\cdot)$ and $H_m^{(1)}(\cdot)$ are the Bessel and Hankel functions, respectively, and the prime denotes differentiation with respect to the argument

$$\begin{aligned} B_{mn}^{\text{slab}} &= (-i)^n i^m J_n(ka) J_m(ka) \Omega_{m+n}^{E(H)} \\ D_{mn}^{\text{slab}} &= (-i)^n i^m J_n(ka) J_m'(ka) \Omega_{m+n}^{E(H)} \end{aligned} \quad (8)$$

where $\Omega_{m+n}^{E(H)}$ are the Sommerfeld integrals given by (25,26) of [5] and

$$A(B, C, D)_{mn}^{\text{shape}} = \frac{1}{4\pi^2} \int_0^{2\pi} \int_0^{2\pi} A(B, C, D)(t, t_s) e^{-imt} e^{int_s} dt dt_s. \quad (9)$$

The set (6) and (7) can be easily converted to a Fredholm second-kind matrix equation, which is solvable numerically with guaranteed convergence. Provided that all intermediate computations have been done with superior accuracy, overall accuracy depends (and, hence, is controlled by) the order of truncation of the matrix equation.

It can be seen that a nondiagonal matrix element is a sum of two components. One component B_{mn}^{slab} or D_{mn}^{slab} is a function of the waveguide and the parameters of the extracted circular resonator only, while the other (e.g., A_{mn}^{shape}) depends on the actual shape of the contour L . Note that as a result of the regularization process, all the integrand functions in (9) are regular, as follows:

$$A(t, t_s) = H_0^{(1)}(k_r R) - H_0^{(1)}\left(2k_r a \left| \sin \frac{t-t_s}{2} \right| \right) \quad (10)$$

$$\begin{aligned} B(t, t_s) &= H_0^{(1)}(k_r R) - H_0^{(1)}\left(2ka \left| \sin \frac{t-t_s}{2} \right| \right) \\ &+ \int_{-\infty}^{\infty} \frac{R^{E(H)}(h)}{\pi g} e^{2ikgb} \left(e^{ik(g(y+y_s)+h(x-x_s))} \right. \\ &\quad \left. - e^{ika(g(\sin t + \sin t_s) + h(\cos t - \cos t_s))} \right) dh \end{aligned} \quad (11)$$

$$\begin{aligned} C(t, t_s) &= kK(t, t_s) \frac{H_1^{(1)}(k_r R)}{R} \\ &+ ka \left| \sin \frac{t-t_s}{2} \right| H_1^{(1)}\left(2k_r a \left| \sin \frac{t-t_s}{2} \right| \right) \end{aligned} \quad (12)$$

$$\begin{aligned} D(t, t_s) &= kK(t, t_s) \frac{H_1^{(1)}(kR)}{R} + ka \left| \sin \frac{t-t_s}{2} \right| \\ &\times H_1^{(1)}\left(2ka \left| \sin \frac{t-t_s}{2} \right| \right) + \int_{-\infty}^{\infty} \frac{iR^{E(H)}(h)}{\pi g} e^{2ikgb} \\ &\times \left(\left(g \frac{dx}{dt} - h \frac{dy}{dt} \right) e^{ik(g(y+y_s)+h(x-x_s))} \right. \\ &\quad \left. - (g \sin t + h \cos t) \right. \\ &\quad \left. \times e^{ika(g(\sin t + \sin t_s) + h(\cos t - \cos t_s))} \right) dh \end{aligned} \quad (13)$$

where $K(t, t_s) = k^2(dx/dt(y-y_s) - dy/dt(x-x_s))$, $g = \sqrt{1-h^2}$, $R = \sqrt{(x-x_s)^2 + (y-y_s)^2}$, and the expressions for coefficients $R^{E(H)}(h)$ can be found in [5]. In particular, the logarithmic singularity in function (10) is cancelled, as it can be shown that

$$\lim_{t \rightarrow t_s} A(t, t_s) = \frac{2i}{\pi} \ln \left| \frac{L(t_s)}{a} \right|. \quad (14)$$

A similar expression holds true for the difference of the first two terms of (11), and the third integral term is a regular function. Therefore, all the integrals (9) can be evaluated accurately by the numerical integration.

(*) not exactly so, see comment below

For the q th incident natural wave, the right-hand sides of (6) and (7) are given by

$$e_m^{E(H)} = f_q^{E(H)} e^{-k\rho_q b} \times \left(i^m J_m(ka)(h_q + \rho_q)^m + \frac{1}{2\pi} \int_0^{2\pi} \times \left\{ e^{k(ih_q x - \rho_q y)} - e^{ka(ih_q \cos t - \rho_q \sin t)} \right\} \times e^{-imt} dt \right) \quad (15)$$

$$\tilde{e}_m^{E(H)} = f_q^{E(H)} e^{-k\rho_q b} \times \left(i^m J'_m(ka)(h_q + \rho_q)^m + \frac{1}{2\pi} \int_0^{2\pi} \times \left\{ \left(ih_q \frac{dy}{dt} + \rho_q \frac{dx}{dt} \right) e^{k(ih_q x - \rho_q y)} - ka(ih_q \cos t + \rho_q \sin t) \times e^{ka(ih_q \cos t - \rho_q \sin t)} \right\} e^{-imt} dt \right) \quad (16)$$

where $f_q^E = \sin(k\gamma_q d)$, $f_q^H = \cos(k\gamma_q d)$, $\rho_q = \sqrt{h_q^2 - 1}$, $\gamma_q = \sqrt{\varepsilon_w - h_q^2}$.

The computational bottleneck of the algorithm based on this scheme is the calculation of the double Fourier expansion coefficients of the IE kernels (9). The fast Fourier transform algorithm combined with the Gauss numerical quadrature [13] was used to speed up the calculations.

C. Far-Field Characteristics and Optical Theorem

In the Fourier integral representation of the Green's function of a dielectric waveguide, the integrand has a number of poles corresponding to the guided waves supported by the dielectric waveguide. Even if the incident field is the fundamental wave, after the scattering from the microdisk, a number of forward and backward waves can be excited in the waveguide. Transmission and reflection coefficients of all the guided waves are obtained by deforming the integration contour in the complex h plane and calculating the residues at the poles $h = \pm h_n$:

$$\left\{ \begin{array}{l} T_n^{E(H)} - \delta_{nq} \\ R_n^{E(H)} \end{array} \right\} = \frac{f_n^{E(H)}}{\pi (N_n^{E(H)})^2} e^{-\rho_n kb} \times \int_0^{2\pi} \left(\sum_{m=0}^{\infty} \psi_m^{E(H)} e^{imt} \right) \cdot e^{-ik(g_n y(t) \mp h_n x(t))} dt. \quad (17)$$

Here, $(N_n^{E(H)})^2$ is the norm of the n th waveguide wave [5, formulas (7) and (8)].

The far-field scattering pattern is evaluated by applying the steepest descent method in the far zone of the scatterer. This brings us to

$$\Phi^{E(H)}(\varphi) = \frac{1}{2\pi} \int_0^{2\pi} \left(\sum_{m=-\infty}^{\infty} \psi_m^{E(H)} e^{imt} \right) \times e^{-ikx(t) \cos \varphi} \times \left(e^{-iky(t) \sin \varphi} + R^{E(H)}(\varphi) \cdot e^{ik(y(t)+2b) \sin \varphi} \right) dt. \quad (18)$$

The far-field characteristics are coupled together by the power conservation law (optical theorem) [17], which has the following form for a microdisk without material losses:

$$1 = P_{\text{tr}} + P_{\text{ref}} + P_{\text{rad}}. \quad (19)$$

On the right-hand side of (19), there are the transmitted, reflected, and radiated power fractions, respectively (i.e., the powers normalized to the power carried by the incident guided wave). Omitting the upper index $E(H)$, they are found as

$$P_{\text{tr}} = \frac{1}{N_q^2} \sum_{n=1(0)}^{Q^{E(H)}} N_n^2 |T_n|^2 \quad (20)$$

$$P_{\text{ref}} = \frac{1}{N_q^2} \sum_{n=1(0)}^{Q^{E(H)}} N_n^2 |R_n|^2 \quad (21)$$

$$P_{\text{rad}} = \frac{2}{\pi N_q^2} \int_0^\pi \left| \Phi^{E(H)}(\varphi) \right|^2 d\varphi. \quad (22)$$

Ensuring the balance of (19) may serve as a partial validation of the numerical code. After this, the optical theorem can be used to minimize the time needed for the computation of P_{rad} by eliminating the time-consuming numerical integration.

III. NUMERICAL RESULTS AND DISCUSSION

A. Horizontal Coupling: Increasing the Coupling Length

The first filter configuration we consider is a bus waveguide and a microdisk in the AlGaAs–GaAs material system, similar to one studied in [4]. The structure is weakly guiding in the vertical direction and strongly guiding in the horizontal direction (in the $x - y$ plane) where the microdisk and waveguide are coupled via an air gap. To take into account the third dimension of the structure and material composition in our 2-D algorithm, we apply the effective-index method. The effective refractive index of the fundamental TE mode at $\lambda = 1.5 \mu\text{m}$ in the $0.45\text{-}\mu\text{m}$ -thick GaAs layer with AlGaAs layers above and below has been used as the bus waveguide and the microdisk refractive index, i.e., $n_w = n_r = 3.2$.

Due to the high-index contrast at the semiconductor–air interface, a very small microdisk-waveguide separation is required to achieve efficient coupling. Fig. 2 demonstrates how the transmittance of the waveguide depends on the gap width. A sharp and deep resonance peak on the transmission characteristic corresponds to the excitation of the WGE_{9,1} mode in the microdisk (the subscripts denote the number of azimuthal and radial variations of the WGM field, respectively). It can be seen that filter characteristics are very sensitive to changes in the air gap width. There are two mechanisms that contribute to this sensitivity. First, the coupling of the bus waveguide to the microdisk changes the natural frequency of the WGM in the resonator [16] and, therefore, shifts the resonance peak. Furthermore, the level of the coupling between the resonator and waveguide decreases (and the transmittance at the resonance increases) as the gap becomes wider. This is a well-known phenomenon [4], [7]–[9], and one of the ways of improving the filter transmission characteristics is to enlarge

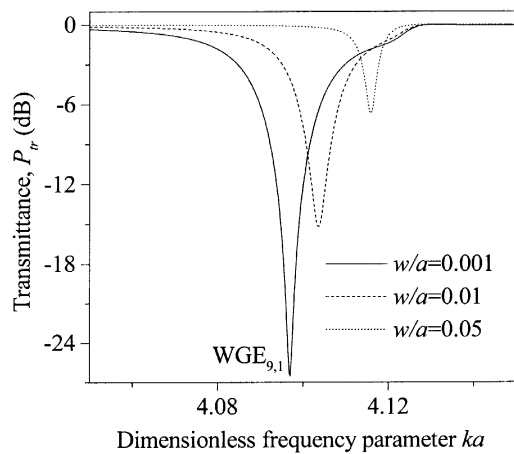


Fig. 2. Transmittance of the circular WGM filter for three values of the width of the air gap between a circular microdisk and waveguide. Monolithic semiconductor integrated circuit: $n_r = n_w = 3.2$, $d/a = 0.22$.

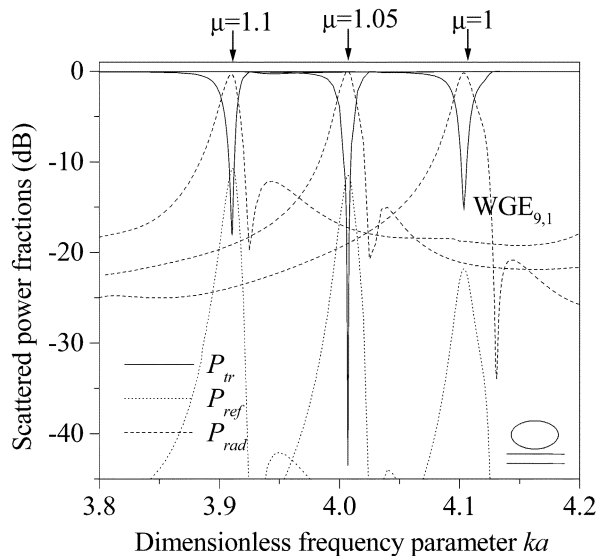


Fig. 3. Transmitted, reflected, and radiated power fractions in the $WGE_{9,1}$ resonance for three horizontally coupled microdisks of different elongation in the monolithic configuration: $n_r = n_w = 3.2$, $d/a = 0.22$.

the coupling length by using elliptical or racetrack resonators. Indeed, Fig. 3 shows how the filter characteristics change if the microdisk is elongated in the horizontal direction. This change of resonator shape both red-shifts the resonance and increases the coupling efficiency. However, further elongation of the microdisk spoils the filter characteristics, a phenomenon that can be explained by a decrease in the quality factor of the WGM in the severely deformed resonator [14], [18].

Let us now consider a hybrid configuration: a $0.45\text{-}\mu\text{m}$ -thick GaAs microdisk and a silica waveguide coupled via an air gap. The structure is formed by mounting the semiconductor disk on a silica-based PLC [11]. In this case, the waveguide is weakly guiding in both vertical and horizontal directions. The effective refractive indexes for the microdisk and waveguide at $\lambda = 1.3\ \mu\text{m}$ are taken as follows: $n_r = 3.2$, $n_w = 1.442$. Fig. 4 presents the transmitted, reflected, and scattered power fractions

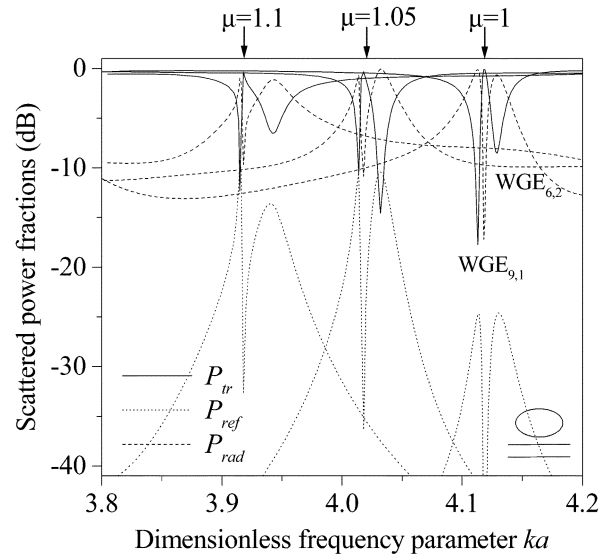


Fig. 4. Transmitted, reflected, and radiated power fractions in the $WGE_{9,1}$ and $WGE_{6,2}$ resonance for three horizontally coupled microdisks of different elongation. Hybrid configuration: semiconductor DR ($n_r = 3.2$) coupled to a silica waveguide ($n_w = 1.442$), $d/a = 0.7$.

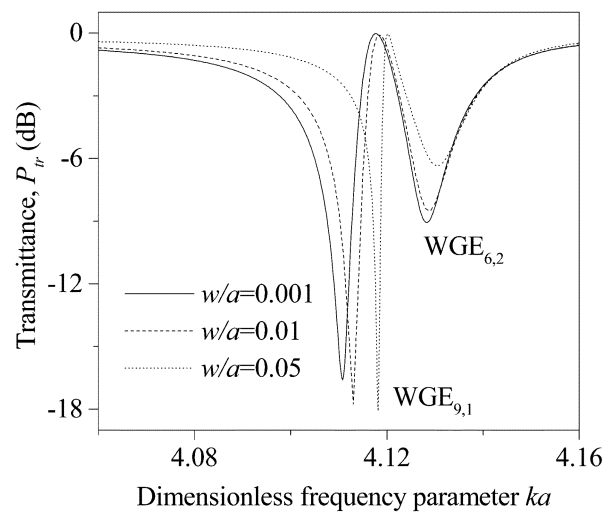


Fig. 5. Transmittance of the circular WGM filter as a function of the width of the air gap between the microdisk and waveguide in the hybrid configuration: $n_r = 3.2$, $n_w = 1.442$, $d/a = 0.7$.

for three different values of the microdisk elongation parameter. It is noted that, in this case, the increase of the coupling length does not lead to an improvement in the filter characteristics. Moreover, a parasitic second-order mode $WGE_{6,2}$ is excited due to a mismatch between the waveguide and microdisk, and the resonance peak associated with this mode becomes even more pronounced with increasing the coupling length. However, such a configuration is much less sensitive to the air gap width (Fig. 5), since the waveguide is now weakly guiding, and its surface wave field penetrates further into the air. An alternative way of tuning the filter in this case is based on exploiting the fact that high-intensity regions in the WGM field of the elongated microdisk are located at the points of the highest curvature of the contour.

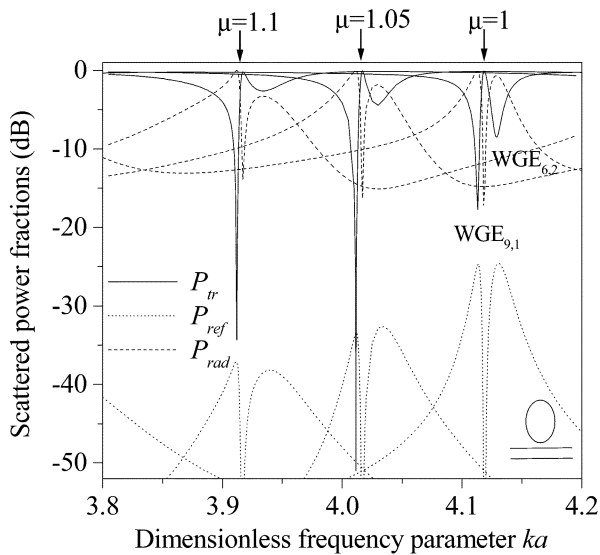


Fig. 6. Transmitted, reflected, and radiated power fractions in the $WGE_{9,1}$ and $WGE_{6,2}$ resonance for three vertically coupled microdisks of different elongation in the hybrid configuration: $n_r = 3.2$, $n_w = 1.442$, $d/a = 0.7$.

B. Vertical Coupling: Exploiting the WGM Features

In circular microdisks, WGMs exist when the light circulates around the rim of the resonator trapped by total internal reflection. The deformation of the microdisk from its circular geometry increases the leakage of the mode field out of the resonator. This leakage occurs at the points of higher curvature of the resonator contour [14], [18]. Therefore, at these points, the WGM field penetrates further into the surrounding media. Indeed, experimentally obtained images of lasing elliptical microdroplets demonstrate high-intensity field regions at the microcavity contour around the major axis of the ellipse [19]. This feature of the WGM field offers an alternative, vertical, coupling of an elliptical microresonator to a straight waveguide. Note, that the term *vertical coupling* is used here to describe a microdisk laterally coupled to a waveguide along its minor axis.

Fig. 6 shows results for the vertical coupling scheme and three different elongations of the microdisk. It can be seen that a slight increase of the ellipse eccentricity leads to more pronounced minima in the transmission characteristics. However, as for the case of horizontal coupling, further deformation of the resonator results in the destruction of the WGM in the microdisk and detuning of the bandstop filter. It should be noted that more severe shape deformations may be required for tuning microdisk filters operating on higher order WGMs.

Comparison of filter characteristics in horizontal and vertical coupling configurations (e.g., Figs. 3 and 7 or Figs. 4 and 6) shows another advantage of the vertical coupling scheme. It can be seen that for horizontally coupled microdisks, the decrease in the transmitted power is accompanied by an increase in the power of the backward-scattered waveguide mode. This can be considered an undesirable effect in the design of optical components such as, e.g., add/drop filters. On the contrary, vertical-coupling configurations provide a good suppression of both the reflected and transmitted modes of the waveguide.

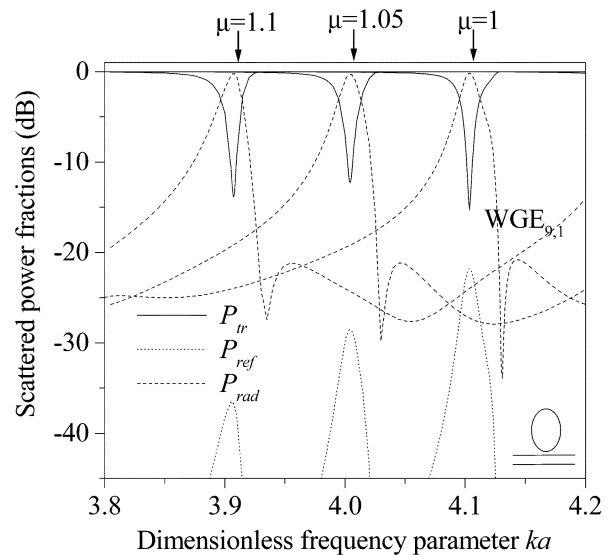


Fig. 7. Transmitted, reflected, and radiated power fractions in the $WGE_{9,1}$ resonance for three vertically coupled microdisks of different elongation in the monolithic configuration: $n_r = n_w = 3.2$, $d/a = 0.22$.

Finally, the magnetic field distributions in the microdisk filters operating on the $WGE_{9,1}$ mode in monolithic and hybrid configurations are shown in Fig. 8(a) and (b), respectively.

C. Effect of Fabrication Imperfections on the Filter Characteristics

During the fabrication process, shape and refractive-index profile imperfections inevitably appear and may lead to detuning of the filter and the spoiling of its characteristics. In this section, we aim to evaluate the effect of such imperfections in order to find the fabrication tolerance.

One of the major factors affecting the filter performance is the surface roughness of the microdisk resonator. We consider a sinusoidal perturbation of the disk radius with corrugation period ν and amplitude δ . The GaAs elliptical microdisk ($n_r = 3.2$, $\mu = 1.05$) is $2.04 \mu\text{m}$ in the minor axis and has an unperturbed resonant frequency of $\lambda_{\text{up}} = 1.595 \mu\text{m}$. Fig. 9 shows how increasing the radius perturbation amplitude shifts the resonant wavelength and causes Q -factor degradation of the $WGE_{9,1}$ mode. It can be clearly seen that the WGM Q factor demonstrates a threshold behavior: it remains large and almost constant up to a certain critical amplitude of the contour deformation, beyond which it decreases rapidly. In [20], the surface roughness of etched GaAs–AlGaAs microdisks and waveguide sidewalls was measured to be of the order of 10 nm, the estimates being obtained from high-magnification scanning electron microscope micrographs and measured propagation losses of the waveguides. It can be seen (Fig. 9) that for a perturbation amplitude of about 10 nm, the Q factor of the microdisk is practically not disturbed.

Observations of this phenomenon for small perturbation amplitudes have been made experimentally and by the FDTD technique for circular microdisks with either deliberately introduced gratings [21] or random perturbations [22] at the resonator rim.

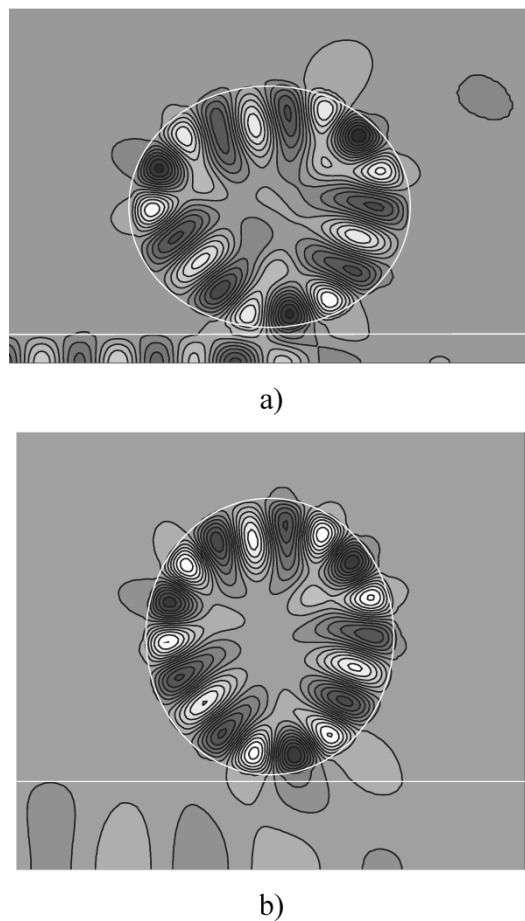


Fig. 8. H_z field patterns of the microdisk filters operating on the $WGE_{9,1}$ mode. (a) Horizontal coupling, $n_r = n_w = 3.2$, $d/a = 0.22$. (b) Vertical coupling, $n_r = 3.2$, $n_w = 1.442$, $d/a = 0.7$.

Evanescent leaking of the WGM out of the resonator due to scattering from the rim imperfections has been found to be not as strong as expected [21]. An explanation offered was that the distance between peaks of the optical modes and the resonator rim was larger than the perturbation amplitude. However, our results (Fig. 9) show that even small resonator boundary perturbations noticeably increase the resonant frequency. This indicates that the WGM shrinks to the inner unperturbed area of the microdisk, and the effective disk radius is diminished to the internal radius of the corrugated disk, $a_{\text{eff}} = a - \delta$. As a result, the resonator Q factor is somewhat insensitive to the low-amplitude arbitrary boundary roughness, but the microdisk resonant frequency can be detuned significantly from its unperturbed value. It should be noted here that specially introduced imperfections tailored to fit a specific field distribution of the microdisk mode can be used to control the Q factor of the mode without changing its resonant frequency [14], [23].

As mentioned previously (see Fig. 2), filters based on circular microdisks evanescently coupled to submicron-width planar waveguides via submicron-width air gaps in the monolithic configuration are very sensitive to the width of this gap. Modern nanofabrication technologies utilizing high-resolution electron-beam lithography and deep reactive ion etching enable the gap width to be as small as $0.1 \mu\text{m}$ [3], [4], [7], [20].

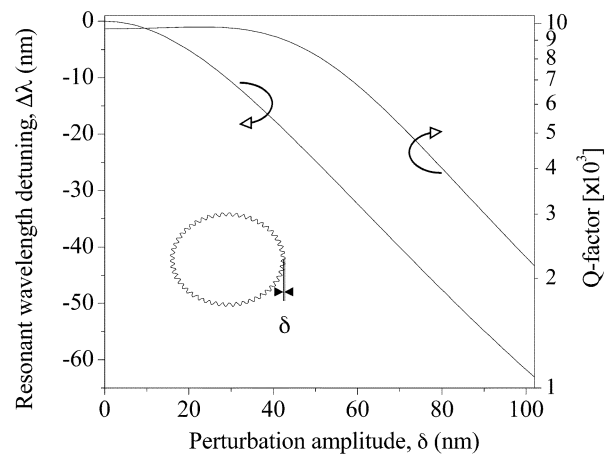


Fig. 9. Resonant wavelength detuning ($\Delta\lambda = \lambda - \lambda_{\text{unp}}$) and Q -factor degradation of the $WGE_{9,1}$ mode of the elliptical microdisk ($n_r = 3.2$, $\mu = 1.05$, $\nu = 30$) as a function of the radius perturbation amplitude.

However, accurate and repeatable fabrication of such narrow gaps is a rather challenging task. The smaller the microdisk, the more difficult it is to control the coupling coefficient. For $2\text{--}5 \mu\text{m}$ -sized microdisks, with free spectral range (FSR) larger than 50 nm , the resolution of the fabrication method is often not high enough to achieve the desired narrow air gaps, and to increase the coupling coefficients, microdisks are fused to bus waveguides [3]. Larger, $5\text{--}10 \mu\text{m}$ -sized resonators with FSR of $20\text{--}50 \text{ nm}$ require air gaps of $0.1\text{--}0.3 \mu\text{m}$, for which the fabrication is more repeatable and tolerant [4], [7], [20]. Here, we consider both coupling designs and study the effect of the air gap width on the filter resonant frequency and coupling efficiency.

First, consider a $2.04\text{-}\mu\text{m}$ GaAs resonator contacting a waveguide. Microdisk or waveguide surface roughness can lead to a poor mechanical contact between them. We simulate this poor-contact effect by introducing a very narrow air gap. If the microdisk is brought to a close-point contact with the waveguide (zero air gap width), the microdisk resonates on its $WGE_{9,1}$ mode at $1.5652 \mu\text{m}$. Fig. 10(a) shows that the increase of the air gap width up to 10 nm causes a blue shift of the resonant frequency by $\sim 3 \text{ nm}$. However, the level of transmittance in the forward direction of the bus waveguide remains very low, with values < 0.05 . It should also be noted that in an add/drop filter configuration, a too-long “fused” section may introduce undesirable scattering losses at the junction [3].

Fig. 10(b) demonstrates the effect of the air gap widening on the performance of a $4.56\text{-}\mu\text{m}$ -diameter GaAs microdisk filter. For a desired gap width of $0.1 \mu\text{m}$, a resonant wavelength of the microdisk $WGE_{24,1}$ mode is $1.5504 \mu\text{m}$. Contrary to the picture of the small fused microdisk detuning (Fig. 10(a)), the shift of the resonant frequency in this case is insignificant, even for a fabrication error in the gap width as large as 100%. However, coupling to the waveguide is weakened, leading to an increase in the transmittance value up to 0.15.

The results of our simulations lead us to a conclusion that, for small resonators fused to bus waveguides, a major fabrication challenge is filter detuning and radiation loss at the junction, while for large evanescently coupled microdisks, it is achieving

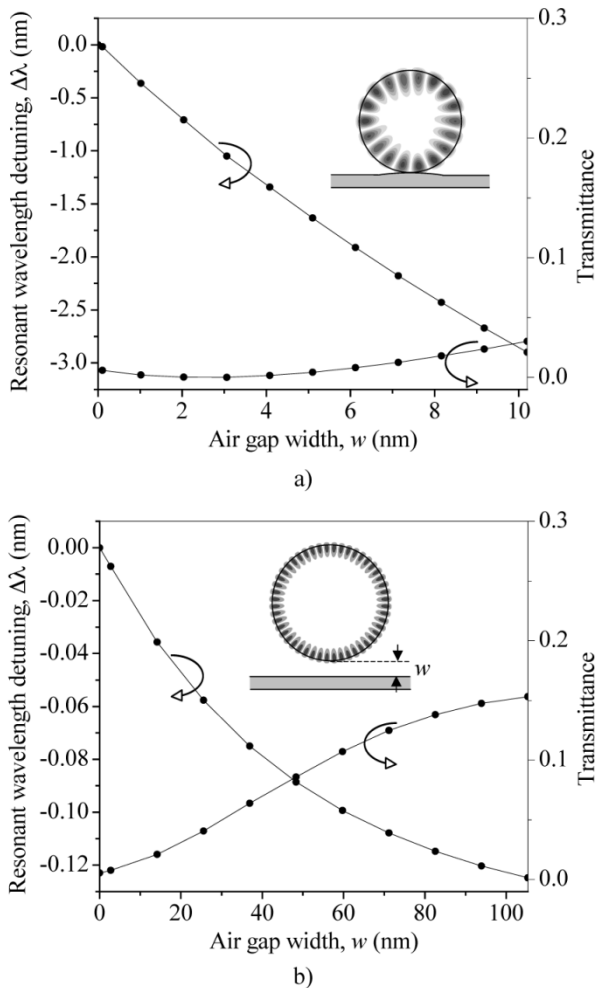


Fig. 10. Resonant wavelength detuning ($\Delta\lambda = \lambda - \lambda_{\text{up}}$) and transmittance of the circular microdisk filters as a function of the microdisk/waveguide air gap width. (a) Small microdisk: $a = 1.02 \mu\text{m}$, $d/a = 0.22$, $n_r = 3.2$, $\lambda_{\text{up}} = 1.5652 \mu\text{m}$. (b) Larger microdisk: $a = 2.28 \mu\text{m}$, $d/a = 0.161$, $n_r = 3.2$, $\lambda_{\text{up}} = 1.5504 \mu\text{m}$.

an optimal coupling to bus waveguides for an efficient power removal from an input channel. We would also like to note that an alternative vertical-coupling configuration has recently been suggested and realized where bus waveguides and the microdisk are located on separate planes [24]. This configuration is fabricated by an epitaxial growth, rather than optical lithography, and enables precise control of coupling coefficients.

IV. CONCLUSION

(*) - see comment below

A computationally efficient algorithm based on the contour IE formulation has been developed to study arbitrary-shaped 2-D WGM microresonators coupled to straight optical waveguides. It has been applied to wavelength-selective filters based upon elliptic microdisk resonators. We have demonstrated how the filter transmission characteristics can be tuned by adjusting the elliptic resonator shape and by providing correct coupling to the bus waveguide. Well-engineered spectral characteristics provide advantages for integration in high-density optical integrated circuits. We have also considered the effect of fabrication imperfections such as surface roughness and variations of the

air gap width on the filter detuning and the coupling efficiency degradation. We emphasize that our results are based on a full Maxwellian analysis and are not restricted in terms of the small contrast of dielectrics or large resonator dimensions.

REFERENCES

- [1] D. Cros and P. Guillon, "Whispering gallery dielectric resonator modes for W-band devices," *IEEE Trans. Microwave Theory Tech.*, vol. 38, pp. 1667–1673, Nov. 1990.
- [2] D. R. Rowland and J. D. Love, "Evanescence wave coupling of whispering gallery modes of dielectric cylinder," *Inst. Elect. Eng. Proc.-J*, vol. 140, no. 3, pp. 177–188, 1993.
- [3] B. E. Little, J. S. Foresi, G. Steinmeyer, E. R. Thoen, S. T. Chu, H. A. Haus, E. P. Ippen, L. C. Kimerling, and W. Greene, "Ultra-compact Si-SiO₂ microring resonator optical channel dropping filters," *IEEE Photon. Technol. Lett.*, vol. 10, pp. 549–551, Apr. 1998.
- [4] S. C. Hagness, D. Rafizadeh, S. T. Ho, and A. Taflove, "FDTD microcavity simulations: Design and experimental realization of waveguide-coupled single-mode ring and whispering-gallery-mode disk resonators," *J. Lightwave Technol.*, vol. 15, pp. 2154–2165, Nov. 1997.
- [5] S. V. Boriskina and A. I. Nosich, "Radiation and absorption losses of the whispering-gallery-mode dielectric resonators excited by a dielectric waveguide," *IEEE Trans. Microwave Theory Tech.*, vol. 47, pp. 224–231, Feb. 1999.
- [6] A. Sakai and T. Baba, "FDTD simulation of photonic devices and circuits based on circular and fan-shaped microdisks," *J. Lightwave Technol.*, vol. 17, pp. 1493–1499, Aug. 1999.
- [7] M. K. Chin and S. T. Ho, "Design and modeling of waveguide-coupled single-mode microring resonators," *J. Lightwave Technol.*, vol. 16, pp. 1433–1446, Aug. 1998.
- [8] R. G. Walker and C. D. W. Wilkinson, "Integrated optical ring resonators made by silver ion-exchange in glass," *Appl. Opt.*, vol. 22, pp. 1029–1035, July 1983.
- [9] M. K. Chin, C. Youtsey, W. Zhao, T. Pierson, Z. Ren, S. L. Wu, L. Wang, Y. G. Zhao, and S. T. Ho, "GaAs microcavity channel-dropping filter based on a race-track resonator," *IEEE Photon. Technol. Lett.*, vol. 11, pp. 1620–1622, Dec. 1999.
- [10] Y. Kogami, Y. Tomabechi, and K. Matsumura, "Resonance characteristics of whispering gallery modes in an elliptic disc resonator," *IEEE Trans. Microwave Theory Tech.*, vol. 44, pp. 473–475, Mar. 1996.
- [11] T. Kitagawa, Y. Akahori, I. Ogawa, and Y. Tohmori, "Hybrid integration technologies using planar lightwave circuits and developed components," *IEICE Trans. Electron.*, vol. E85-C, pp. 1009–1017, Apr. 2002.
- [12] G. L. Hower, R. G. Olsen, J. D. Earls, and J. B. Schneider, "Inaccuracies in numerical calculations of scattering near natural frequencies of penetrable objects," *IEEE Trans. Antennas Propagat.*, vol. 41, pp. 982–986, July 1993.
- [13] A. I. Nosich, "The method of analytical regularization in wave-scattering and eigenvalue problems: foundations and review of solutions," *IEEE Antennas Propagat. Mag.*, vol. 41, pp. 34–49, Mar. 1999.
- [14] S. V. Boriskina, T. M. Benson, P. Sewell, and A. I. Nosich, "Highly efficient design of specially engineered whispering-gallery-mode laser resonators," *Optical Quantum Electron.*, vol. 35, no. 1, pp. 545–559, Mar./Apr. 2002.
- [15] D. Colton and R. Kress, *Integral Equation Method in Scattering Theory*. New York: Wiley, 1983.
- [16] S. V. Boriskina, T. M. Benson, P. Sewell, and A. I. Nosich, "Effect of a layered environment on the complex natural frequencies of 2D WG-mode dielectric-ring resonators," *J. Lightwave Technol.*, vol. 20, pp. 1563–1572, Aug. 2002.
- [17] P. G. Petropoulos and G. A. Kriegsmann, "Optical theorems for electromagnetic scattering by inhomogeneities in layered dielectric media," *IEEE Trans. Antennas Propagat.*, vol. 39, pp. 1119–1124, Aug. 1991.
- [18] J. U. Nöckel, A. D. Stone, and R. K. Chang, "Q spoiling and directionality in deformed ring cavities," *Opt. Lett.*, vol. 19, pp. 1693–1695, 1994.
- [19] S. A. Backes, A. P. Heberle, J. R. A. Cleaver, and K. Köhler, "Shape dependence of emission from microdisk lasers," *Physica Status Solidi B*, vol. 204, no. 1, pp. 581–583, 1997.
- [20] V. Van, P. P. Absil, J. V. Hryniewicz, and P.-T. Ho, "Propagation loss in single-mode GaAs-AlGaAs microring resonators: Measurement and model," *J. Lightwave Technol.*, vol. 19, pp. 1734–1738, Nov. 2001.
- [21] A. F. J. Levi, R. E. Slusher, S. L. McCall, J. L. Glass, S. J. Pearton, and R. A. Logan, "Directional light coupling from microdisk lasers," *Appl. Phys. Lett.*, vol. 62, pp. 561–563, Feb. 1993.

- [22] B.-J. Li and P.-L. Liu, "Numerical analysis of microdisk lasers with rough boundaries," *IEEE J. Quantum Electron.*, vol. 35, pp. 791–795, May 1997.
- [23] M. Fujita and T. Baba, "Proposal and finite-difference time-domain simulation of whispering gallery mode microgear cavity," *IEEE J. Quantum Electron.*, vol. 37, pp. 1253–1258, Oct. 2001.
- [24] K. Djordjev, Se.-J. Choi, Sa.-J. Choi, and P. D. Dapkus, "High-Q vertically coupled InP microdisk resonators," *IEEE Photon. Technol. Lett.*, vol. 14, pp. 331–333, Mar. 2002.



Svetlana V. Boriskina (S'96–M'00) was born in 1973 in Kharkov, Ukraine. She received the M.Sc. degree in radio physics (with honors) and the Ph.D. degree from Kharkov National University, Kharkov, Ukraine, in 1995 and 1999, respectively.

From 1997 to 1999, she was a Researcher in the School of Radio Physics, Kharkov National University, and in 2000, a Royal Society—NATO Postdoctoral Fellow in the School of Electrical and Electronic Engineering, University of Nottingham, Nottingham, U.K., where she is currently a Research Associate.

Her research interests are in integral equation methods for electromagnetic wave scattering and eigenvalue problems in layered media, with applications to microwave and optical waveguides, dielectric resonators, and antennas.



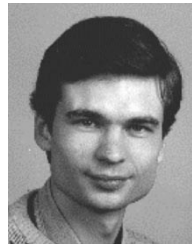
Trevor M. Benson (M'95–SM'01) was born in 1958 in Sheffield, U.K. He received the First Class honors degree in physics and the Ph.D. degree in electronic and electrical engineering from the University of Sheffield, Sheffield, U.K., in 1979 and 1982, respectively.

After spending more than six years as a Lecturer at University College Cardiff, he joined the University of Nottingham, Nottingham, U.K., as a Senior Lecturer in electrical and electronic engineering in 1989.

He was promoted to the posts of Reader in photonics

in 1994 and Professor of optoelectronics in 1996. His present research interests include experimental and numerical studies of electromagnetic fields and waves, with particular emphasis on propagation in optical waveguides and lasers, silicon-based photonic circuits, and electromagnetic compatibility.

Dr. Benson received the Clark Prize in Experimental Physics from the University of Sheffield in 1979.



Phillip Sewell (S'88–M'91) was born in 1965 in London, U.K. He received the B.Sc. degree in electrical and electronic engineering (first-class honors) and the Ph.D. degree from the University of Bath, Bath, U.K., in 1988 and 1991, respectively.

From 1991 to 1993, he was an S.E.R.C. Postdoctoral Fellow at the University of Ancona, Italy. Since 1993, he has been a Lecturer, and from 2001 a Reader, in the School of Electrical and Electronic Engineering, the University of Nottingham, Nottingham, U.K. His research interests

involve analytical and numerical modeling of electromagnetic problems, with application to optoelectronics, microwaves, and electrical machines.



Alexander I. Nosich (M'94–SM'95) was born in 1953 in Kharkov, Ukraine. He graduated from the School of Radio Physics of the Kharkov National University, Kharkov, Ukraine, in 1975 and received the Ph.D. and D.Sc. degrees in radio physics from the same university in 1979 and 1990, respectively.

Since 1978, he has been on research staff of the Institute of Radio-Physics and Electronics (IRE) of the Ukrainian Academy of Sciences, Kharkov, Ukraine. From 1992 to 2002, he held research fellowships and visiting professorships in Turkey, Japan, France, and

Italy. Currently, he is a leading Scientist in the Department of Computational Electromagnetics, IRE. His research interests include methods of analytical regularization, free-space and open-waveguide scattering, complex-mode behavior, radar cross-sectional analysis, and antenna simulation.

(*) The field representation in terms of only the single-layer potential that leads to IEs (3) and (4) is not the most general one. The same is true for the representation in terms of only the double-layer potential. Either of these representations leads to the appearance of the spurious (real-valued) eigenvalues of resulting IE that spoil the algorithm because the IE condition number has poles at the spurious-eigenvalue frequencies. The lowest of them, as can be easily found, lies near to the value where the largest "diameter" of the scatterer approximately equals to one-half of the free-space wavelength. The severity of associated numerical error depends, however, on the details of the IE discretization scheme used.

If it is a MAR-based scheme as in the current paper, then the error is inacceptably large only in the domain whose width is of the same order as MAR's error and can be squeezed to machine-precision width by taking the matrix truncation order larger.

However if the IE is discretized using a rougher scheme like a BEM or Galerkin MoM with local basis functions, then the domains of huge errors are much wider and overlap one another at the frequencies slightly larger than the first spurious-eigenvalue frequency. This makes any computations with such an algorithm completely senseless.

The full remedy is the use of the Muller IE which is completely equivalent to the original boundary-value problem and thus free of spurious eigenvalues.